Potential dependence of step and kink energies on Au(100) electrodes in sulfuric acid

Sabine Dieluweit, Harald Ibach and Margret Giesen*

Forschungszentrum Jülich, Institut für Schichten und Grenzflächen ISG 3, D 52425 Jülich, Germany. E-mail: m.giesen@fz-juelich.de

Received 19th November 2001, Accepted 21st January 2002
First published as an Advance Article on the web 29th April 2002

Using electrochemical STM we studied monolayer high Au islands on Au(100) electrodes in sulfuric acid as a function of the electrode potential. We made use of theoretical and experimental methods recently developed for UHV experiments on metal islands. It is demonstrated that these models are likewise applicable to islands on metal electrodes in a liquid environment. From a quantitative analysis of the equilibrium island shape and of the island shape fluctuations we determined the step free energy (line tension) as a function of orientation and the kink energy, and the dependence of these quantities on the electrode potential. In a first approach to a theoretical understanding the electrostatic contributions to the line tension are considered. It is concluded that these contributions should add significantly to the observed variation with the potential. This fails however to provide essential features of the experimental result.

1. Introduction

The electrochemical scanning tunnelling microscope (EC-STM)[1,2] has become a powerful tool for studying electrode surfaces in a liquid environment. Its capabilities have been proven by many (partially atomically resolved) studies of the metal deposition on metal electrodes,[3–14] and by studies of the structure of the metal interface (*e.g.* surface reconstruction and adlayer formation).[15–23] Very recently, there have been new efforts to investigate the atomic energy parameters at the solid/liquid interface by EC-STM[24–35] (for a recent review see *e.g.* ref. 36). In these studies theoretical methods based on concepts of statistical physics which were originally developed for the analysis of step and island dynamics on surfaces in ultra-high vacuum (UHV) were applied to deduce quantitative values for diffusion barriers and defect formation energies (see ref. 36 for an overview). The results published so far, however, merely represent the beginning of systematic investigations. It is presumably because of specific difficulties of these studies in a liquid environment (compared to UHV) that only a few scientific groups have focused their interest on systematic and quantitative studies of atomic energy parameters on metal electrodes: Firstly, in contrast to UHV, the electrode potential becomes an additional parameter, besides temperature, which influences the electrode surface on the atomic scale. Secondly, while surfaces in UHV are free of adsorbates, electrolyte ions are always present at the solid/liquid interface and play a crucial role in interfacial energies (see *e.g.* ref. 37). A particular problem in the transfer of the concepts developed in UHV is that some of the methods require temperature dependent measurements, and the temperature range accessible in EC-STM cells is rather limited. A further problem is that STM electrochemical cells do not necessarily provide stable electrode potential conditions due to the geometry of the small cell, the reference and counter electrodes. Hence, the sample potential is

associated with a relatively large uncertainty and it is quite a challenge to achieve reproducible measurements. Last but not least, many scientists are still concerned about a possible influence of the tunnelling tip. This concern applies to investigations at either the solid/liquid or at the solid/vacuum interface. In most cases, however, the tip influence can be ruled out if special care is taken during STM recording.

The importance of defects and their contribution to interfacial energies is known from classical electrochemistry studies.[38,39] Since steps change the local workfunction on surfaces[40] one may *e.g.* expect that steps on electrode surfaces will shift the potential of zero charge (pcz). Furthermore, steps serve as preferred adsorption sites for electrolyte ions.[41] First studies on the balance between interfacial and electrochemical energies were performed by Xia *et al.*[42] who discussed the relation between surface and electrochemical energy in Cu clusters investigations on Au(111) in electrolyte. Detailed quantitative information on the contribution of steps and kinks to the electric properties of the double layer, however, is still missing. *Vice versa*, the effect of the electric double layer and adsorbates on the energetic parameters of the steps is still largely unknown . It is the goal of this paper to present for the first time experimental data on the step free energy (line tension) on a metal electrode as a function step orientation and electrode potential, and on the energies of kink sites in steps. We determine the step free energy and the kink formation energy for Au(100) electrodes in sulfuric acid by studying island equilibrium shapes and island shape fluctuations. The paper is organised as follows. In section 2 we will briefly review the basic theoretical concepts necessary to analyse island shapes and shape fluctuations and we will describe the experimental set-up. The experimental results will be presented in section 3 and they will be discussed in section 4. The paper ends with a summary in section 5.

2. Theoretical concepts and experimental set-up

2.1. Theoretical concepts to analyse island equilibrium shapes

The theoretical concepts are based on methods known from statistical physics and thermodynamics and have been published previously (for a review see ref. 36). We emphasise that these concepts can be applied to either interface, solid/vacuum or solid/liquid, since they merely require that the system is in thermodynamic equilibrium. The latter is determined by the minimum in the Gibbs energy which itself is related to interfacial energies (as *e.g.* surface energies and step energies) and to formation energies (as *e.g.* kink energies). Compared to UHV, these quantities may of course be altered by the presence of the liquid. The change in the energetic parameters, however, will merely result in characteristic modifications of the equilibrium state of the solid/liquid interface. It is precisely these modifications in which we are interested. In the following, we briefly recall the basic equations necessary to analyse the island data.

(a) Equilibrium island shape, Wulff-construction and determination of relative step energies. The equilibrium shape of an island is given by the dependence of the step free energy $\beta(\theta)$ on the polar angle θ. By means of the so-called "Wulff-construction"[43] the equilibrium shape can be directly derived from $\beta(\theta)$. *Vice versa*, if the equilibrium shape is known from experiment, the angle-dependence of θ is obtained from the equilibrium shape by means of the "inverse" Wulff-construction,[44] which is discussed for two-dimensional islands in ref. 45. In this construction, the step free energy is obtained, save for a constant factor. Hence, the relative step free energies may be determined. The resulting variation of β with the angle θ may thence be displayed by plotting $\beta(\theta)/\beta(0)$, where $\beta(0)$ serves as the reference and will be chosen in the following to be the energy of a step along the $\langle 110 \rangle$-direction corresponding to the centre of the quasi-straight segments of the island shape.

The ratio $\beta(45°)/\beta(0°)$† (which is the step free energy of the corner region divided by the step free energy of the $\langle 110 \rangle$-step for fcc (100) surfaces) and is called the "aspect ratio". The aspect ratio is

† For fcc (111) surfaces the corresponding aspect ratio is denoted as $\beta(30°)/\beta(0°)$. Note, however, that the "aspect ratio" for (111) surfaces is frequently defined as the ratio between the step free energies for the two different step types (A- and B-type steps) forming a (100)- and a (111)-microfacet with the underlying terrace, respectively: $\beta_A/\beta_B = \beta(60°)/\beta(0°)$.

identical to the ratio of the corresponding radii at $\theta = 45°$ and 0°, respectively, as obtained from the equilibrium shape. The aspect ratio may lie between two limits: Firstly, when the island shape is a perfect square, then $\beta(45°)/\beta(0°) = \sqrt{2}$. And secondly, for a perfect circular island the aspect ratio is equal to 1 and the step free energy does not depend on the polar angle θ.

(b) Determination of kink and absolute step energies by studies of the local curvature of island shapes. In ref. 45 we showed that the curvature of the equilibrium shape of an island at $\theta = 0$ is related to the step free energy $\beta(\theta = 0)$ *via*

$$y(x=0)\left.\frac{\partial^2 y}{\partial x^2}\right|_{x=0} \tilde{\beta}(\theta=0) = \beta(\theta=0). \tag{1}$$

The angle θ is chosen such that $\theta = 0$ corresponds to the $\langle 110\rangle$-orientation of a step segment in the island perimeter. The corresponding cartesian coordinates x and y of the island perimeter are defined such that $x = 0$ for $\theta = 0$, hence $y''(x = 0)$ represents the curvature of the island at $\theta = 0$. The step edge stiffness $\tilde{\beta}(\theta)$ of the island perimeter at a given polar angle θ is given by[46]

$$\tilde{\beta} = \beta + \frac{\partial^2 \beta}{\partial \theta^2} \tag{2}$$

The step edge stiffness $\tilde{\beta}$ may be expressed in terms of the diffusivity b^2:[46]

$$\tilde{\beta} = \frac{k_B T}{b^2} a_{\|} \tag{3}$$

where $a_{\|}$ is the distance between the centres of the atoms along $\langle 110\rangle$. In the limit of low temperatures (*i.e.* for kinks of monatomic length), the diffusivity b^2 may be approximated by the kink concentration[46] such that

$$\tilde{\beta}(\theta=0) = \frac{k_B T}{b^2} a_{\|} \approx \frac{k_B T a_{\|}}{2a_{\perp}^2 \exp\left(-\frac{\varepsilon}{k_B T}\right)} \tag{4}$$

where ε is the kink energy and $a_{\perp}$ the distance between atomic rows perpendicular to $\langle 110\rangle$ Inserting eqn. (4) into eqn. (1) and using $a_{\|} = a_{\perp}$ for (100) surfaces, one has[45]

$$y(x=0)\left.\frac{\partial^2 y}{\partial x^2}\right|_{x=0} k_B T \approx 2\beta a_{\|} \exp\left(-\frac{\varepsilon}{k_B T}\right) \tag{5}$$

From eqn. (5) it becomes obvious that temperature variable data on the local curvature and the island radius at the centre of $\langle 110\rangle$-oriented island segments (*i.e.* for $x = 0$) are, in principle, sufficient to determine the kink and the step energy. In an Arrhenius plot of the left-hand side of eqn. (5) the kink energy is given by the slope, and the step energy by the intersection.‡ If temperature-variable data is not available, either the kink energy or the step energy must be independently determined from a different measurement. The kink energy may be measured by analysing the (purely!) spatial equilibrium fluctuations of monatomic steps (for recent reviews see ref. 36 and 47). Frequently, and so for the Au(100) surfaces in an electrolyte at 300 K, spatial step fluctuations are intermixed with time dependent fluctuations and the corresponding analysis in terms of the kink concentration cannot be performed. Absolute values for β, on the other hand, may be obtained from the analysis of the equilibrium fluctuations of the island shape which is discussed in the next section.

‡ One should emphasize, however, that an Arrhenius plot of eqn. (5) requires a large data set (based on the analysis of approximately 100 000 to 200 000 island shapes total for 15–20 different temperatures). Even if such a large data base were available, the kink energy might be determined rather accurately while the error bar of the step energy may still be quite large (~30%). As is discussed in the following, it is better to determine the step energy from the island shape fluctuations.

(c) Determination of step energies by island shape fluctuation studies. The relation between the magnitude of island shape fluctuations and the mean step free energy is derived using a capillary mode analysis of Khare and Einstein[48] which was applied to island fluctuation studies by Schlößer *et al.*[49] The theory was extended to islands of arbitrary shape and applied to Cu(100), Cu(111) and Ag(111) surfaces in UHV by Steimer *et al.*[50] At equilibrium, the island shape represents a minimum in the free energy of the island. Due to the island edge fluctuations, the time average of the total free energy is larger since each normal mode of the fluctuations carries the additional free energy k_BT. For an island with mean radius $\bar{r}$, the fluctuation function $\langle G(\bar{r})\rangle$, which represents the time average of the deviations of the island shape from its equilibrium shape, is given by

$$\langle G(\bar{r})\rangle_t = \frac{3k_BT}{4\pi}\frac{\bar{r}}{\bar{\beta}}, \tag{6}$$

where $\bar{\beta}$ is the mean step free energy along the island perimeter. Details of the derivation and the validity of eqn. (6) in specific limits are given in ref. 50.

Any potential dependence of the equilibrium shape, of the aspect ratio, of the island edge curvature and of the shape fluctuation function is determined by the dependence of both the kink energy ε and the step energy β on the electrode potential. We neglect here any shift of the electrode potential with temperature, since the potential shift in the accessible temperature range (5–60 °C) for aqueous electrolytes is rather small.

2.2. Experimental set-up

The measurements were performed with the electrochemical version of the Topometrix TMX 2010 Discoverer STM. Our instrument was modified to enable temperature variable STM recording with high thermal drift stability and is described in detail elsewhere.[29,51] In the studies reported here, however, all experimental results were obtained at 297 K. The tip and the sample potential are independently controlled *via* a bipotentiostat.

Our studies on the island shape were performed on Au(100) single crystal electrodes which were cut by spark erosion from a single crystal rod, oriented by diffractometry and polished to the desired orientation to within 0.1°, which is the accuracy of high-quality single crystals. The accuracy is naturally limited by the mosaic structure of the crystal. Prior to experiment, the Au(100) electrode was heated in a hydrogen atmosphere and then flame annealed for about 5 min to about 900 °C. The temperature was visually controlled by the color of the annealed crystal. After thoroughly rinsing the cell with Milli-Q water, the crystal was mounted in the electrochemical STM cell which was connected to the bipotentiostat. The crystal surface was then brought in contact with the electrolyte under potential control at −150 mV *vs.* SCE. This was visually checked at the beginning of each STM experiment by the presence of the well-ordered quasi-hexagonal reconstruction of the clean Au(100) surface.[52–54] The mean terrace width of the crystal was of the order of 100 nm. As an electrolyte, we used suprapure H_2SO_4 (Merck) and Milli-Q water from a Millipore Elix 3 and A10 Gradient system (18.2 MΩ cm^{-1}; organic contents < 3 ppb). In all experiments, the concentration of the electrolyte was 50 mM.

The tunnelling tips used in the experiments were etched from polycrystalline tungsten wires and coated with polyethylene to avoid Faraday currents at the foremost part of the tip.[55] We used a tunnelling current of 2 nA and the tip bias was held constant at −0.07 V *vs.* SCE to avoid oxidation of the tungsten tip. This means the tunnelling resistance varied between 0.19 and 0.39 GΩ for electrode potentials between +300 and +700 mV *vs.* SCE. The typical time per image was about 60 s and the STM images were recorded with a 400 × 400 pixel resolution in the constant current mode using a scan width of 180 nm. High-purity, flame-annealed Pt wires (Goodfellow, 99.999%) served as counter and quasi-reference electrodes. In the following, the electrode potentials of the metal sample are, however, given with respect to the saturated calomel electrode (SCE). As a caveat we emphasise that the electrode potentials denoted here are the nominal values given by the bipotentiostat. After each experiment we checked the potential by measuring a cyclic voltamogramm in the STM cell. Still we cannot exclude that the potential values as denoted here might deviate from the real potential by about ±20–30 mV due to possible shifts in the potential during experiment.

For the experimental analysis the monolayer high Au islands were created by stepping the electrode potential from −150 mV *vs.* SCE where the crystal was immersed in the electrolyte to

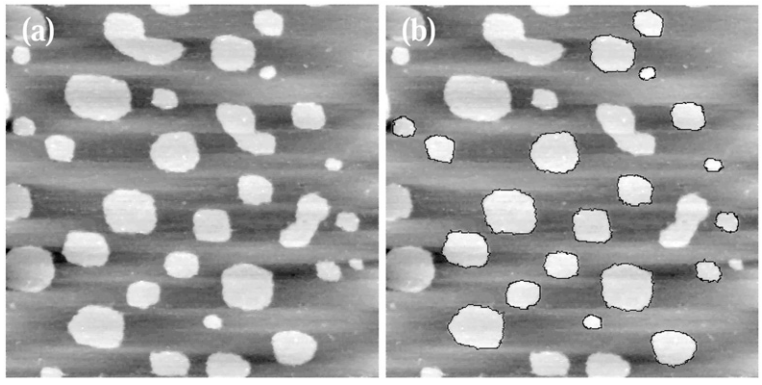

Fig. 1 STM images of Au islands on Au(100) in 50 mM H_2SO_4 at +400 mV *vs*. SCE (a) before and (b) after running the computer code to find the perimeter (black curves) of various islands used for the analysis. Scan area 171×171 nm^2.

potentials higher than +280 mV *vs.* SCE where the (hex)-surface reconstruction is lifted and monolayer high islands nucleate on the less dense (1×1) surface.[16] The experiments were performed at electrode potentials between +300 and +700 mV *vs.* SCE. At the beginning of our experiments we frequently observed the ordered incommensurate sulfate adlayer first reported by Kolb and co-workers.[15,56] The possibility of observing the ad-structure in STM investigations has been attributed to the use of a large tunnelling resistance and clean electrolytes.[56] About 30 min after stepping to potentials higher than +280 mV in which we allowed for the stabilisation of the system prior to measurement, the sulfate structure was not observed. We attribute the vanishing of the sulfate structure to disorder caused by the start of oxygen contamination of the electrolyte in the open STM cell and to the scanning process.

The island shapes of individual islands in the STM images are determined by a special computer code which searches for the maximum slope in the grey scale in an STM image. Starting at a distinct point in the centre of an island, the program finds the radius of an island for a given polar angle. The accuracy of the overall shape is given by the step width between individual polar angles which can be chosen to be a minimum value of 1° (in other words by the number of base points, at maximum 360), by the pixel noise and by the noise in the STM image. In the experiments reported here, the island shapes were determined using 200 base points (*i.e.* 200 number pairs consisting of the island radius and the corresponding polar angle). Fig. 1 shows (a) an STM image of Au islands on Au(100) in 50 mM H_2SO_4 at +400 mV *vs.* SCE before and (b) after the islands has been found and marked (black lines) by the computer code. From Fig. 1(b) one sees that the black lines reflect the general shape and almost all the small features in the island perimeter. Nevertheless, small deviations may be introduced by the computer code which may cause a systematic noise level in the data. If one compares, however, the noise of the perimeter found with the actual shape fluctuations of the islands, one finds that the error in the island area introduced by the computer determined perimeter is of the order of 1% (this corresponds to errors in the island shape radius of the order of 0.5%).§

Depending on the chosen electrode potential, good experimental conditions lasted for from 30 min up to 2 h. Then, generally, contamination of the electrolyte in the open STM cell became visible and the measurements were stopped.

§ Note that in Fig. 1 the island shapes merely reflect a snap shot of the shapes of the fluctuating islands. The shapes of individual islands are different in subsequent frames. The equilibrium shape may only be determined by averaging the measured shapes over many STM images. Note also that some of the shapes in Fig. 1 are caused by coalescence events between islands in close proximity. Such shapes were not considered for the analysis. In later frames, however, these coalesced islands recover the equilibrium shape again.

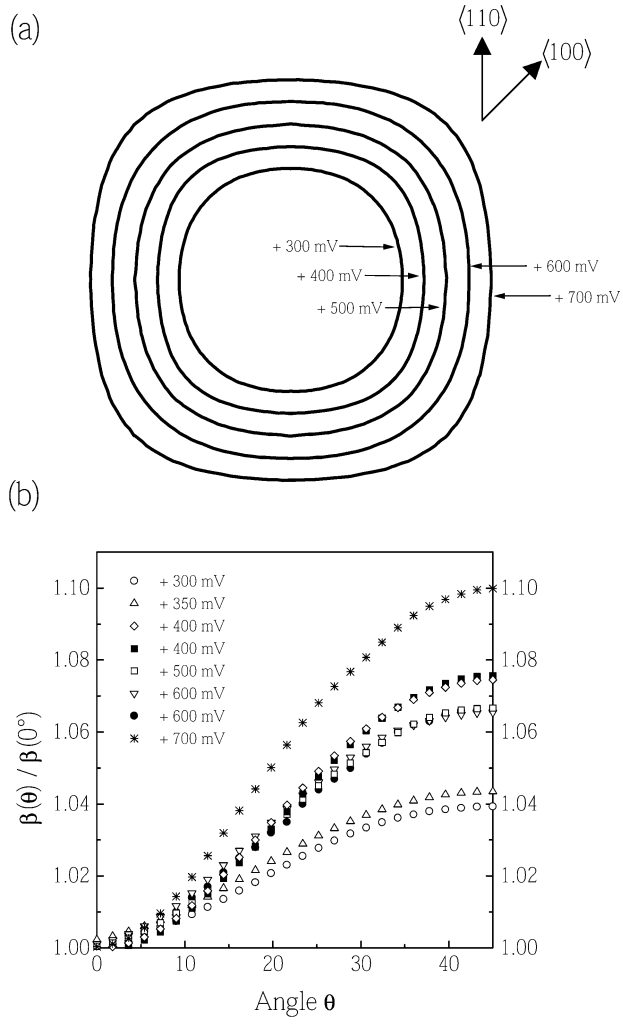

Fig. 2 (a) Equilibrium shapes measured from 100–500 individual Au islands for different electrode potentials. (b) Dependence of the step free energy on the orientation θ obtained from an inverse Wulff plot on the equilibrium shapes.

3. Experimental results

3.1. Equilibrium shape and island edge curvature

Fig. 2 shows (a) the equilibrium shape and (b) the dependence of the step free energy on the orientation $\beta(\theta)/\beta(0°)$ for different electrode potentials after averaging over 100–500 individual island shapes from long STM image series.¶ The equilibrium shape changes as the potential increases. Close to the (hex) $\rightarrow (1 \times 1)$ phase transition, the island shape is almost circular. The change in the island shape is associated with an increase in the aspect ratio $\beta(45°)/\beta(0°)$ which, however, does not seem to be a monotonic increase. This becomes obvious by inspection of the data sets obtained at +400 and +600 mV *vs.* SCE. For both electrode potentials, we have analysed independent data sets from different dates, different single crystals and with new electrolyte

¶ STM movies may be downloaded from http://www.fz-juelich.de/isg/isg3/Giesen/ag-giesen1.htm#Movies.

Table 1 Aspect ratio $\beta(45°)/\beta(0°)$ and curvature yy'' (eqn.(5)) as obtained from the island shape as a function of the electrode potential. The column "yy'' (mean)" denotes the averaged data plotted in Fig. 3 if more than one data point was available at a distinct potential

Electrode potential/mV *vs.* SCE	Aspect ratio $\beta(45°)/\beta(0°)$	yy''	yy'' (mean)
300	1.036	0.8857	0.8005
300	1.039	0.7153	–
350	1.043	0.6456	0.6456
400	1.076	0.6148	0.6242
400	1.077	0.6335	–
500	1.066	0.6205	0.5878
500	1.067	0.5550	–
600	1.065	0.7153	0.6494
600	1.067	0.6457	–
600	1.069	0.5872	–
700	1.100	0.4245	0.4245

solutions. The first striking result is that the individual data sets for +400 and +600 mV are very reproducible. For each potential, the data sets obtained from independent experiments yield almost the same result and are indistinguishable within the statistical noise (Table 1). The second striking observation is, however, that the aspect ratio as measured from the equilibrium shape at +400 mV is larger than that obtained at +600 mV. The aspect ratio measured at +700 mV, on the other hand, is again much larger than for all the other data sets obtained at lower potentials. The results for $\beta(45°)/\beta(0°)$ are also summarised in Fig. 3 which shows the variation of the aspect ratio with electrode potential as squares.

Similar to the aspect ratio, the measured curvature form the quasi-straight island segments displays a non-monotonic trend as a function of the electrode potential. Fig. 4 shows a plot of $y(x=0)\cdot\partial^2 y/\partial x^2|_{x=0}$ versus the electrode potential. The value of $y(x=0)\cdot\partial^2 y/\partial x^2|_{x=0}$ was obtained from a Taylor expansion fit to the equilibrium shape ±15° around the position $x=0$ ($\equiv\theta=0°$).‖ The experimental data (squares) for $y(x=0)\partial^2 y/\partial x^2|_{x=0}$ are the mean values at a given potential. The error bars represent the statistical error bars if more than one data point for $y(x=0)\partial^2 y/\partial x^2|_{x=0}$ was available. The values obtained for the island edge curvature at $x=0$ for the various potentials are also given in Table 1.

3.2. Island shape fluctuations

Fig. 5 displays the time average of the deviation function $\langle G(\bar{r})\rangle$, as defined in eqn. (6) *vs.* the product of the island radius and the temperature for four different electrode potentials. Since the islands used for the analysis undergo coarsening *via* Ostwald ripening, the island area changes during STM recording. Therefore we have divided the analysed islands into sub-sets of islands of about equal area where we allowed area deviations of ±10% at the maximum. The individual sub-sets contained 3–40 islands and were analysed with respect to the shape fluctuations separately, where we defined the fluctuations as a deviation from the mean shape of the entire set. Each data point in Fig. 5(a)–(d) corresponds to one of these sub-sets. From a linear fit** to the data in Fig.

‖ We have also checked the results for smaller angle deviations. The obtained curvature values do not change if the data set is large and the noise in the data for the equilibrium shape is small. For not so large data sets, the value of the curvature systematically decreases with decreasing angle variation, however, the error bars for the obtained value of yy'' become large because of the small number of base points for the Taylor expansion fit. In order to get information about the general trend of the potential dependence of the curvature we discuss merely the results for yy'' obtained for one distinct angle variation. The most reliable appeared to be the data analysed with $\Delta\theta=\pm15°$.

** The fit was forced to intersect the y-axis at zero. This is reasonable since the pixel noise is negligible compared to the magnitude of the shape fluctuations.[49]

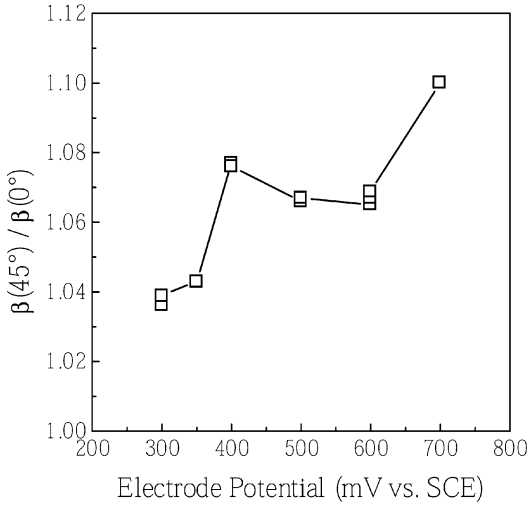

Fig. 3 Measured aspect ratios *versus* electrode potential.

5(a)–(d) we find the slope from which we determine the mean step free energy $\bar{\beta}$ according to eqn. (6). Only a few of the island data obtained from an individual experiment at a distinct electrode potential were sufficiently large to analyse the island shape fluctuation function. If different individual data sets at one potential were available, we have therefore combined the data in one view graph for $\langle G(\bar{r})\rangle$, as displayed in Fig. 5. The slope and the mean step free energy were then determined from the combined plot. The results are displayed in Table 2. For $U = +700$ mV, $\bar{\beta}$ has larger error bars which are indicative of a smaller data base for the shape fluctuation analysis in this case. In Fig. 6, we have plotted the results for the mean step free energy *vs.* the electrode potential as squares.

With the data for the mean step free energy as given in Fig. 6 and Table 2, we have determined the corresponding kink energy ε *vs.* the electrode potential using eqn. (5). The results are given in

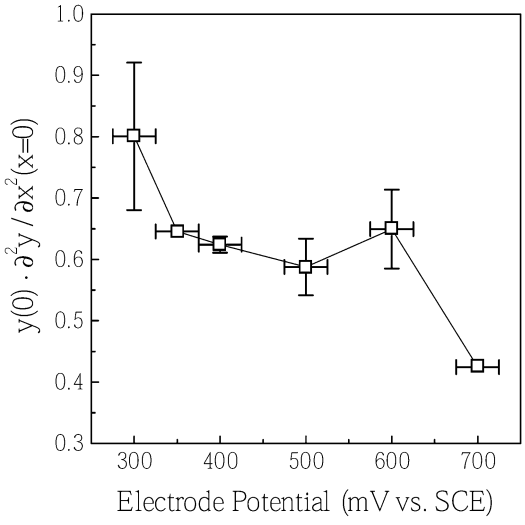

Fig. 4 Curvature yy'' of the quasi-straight island edge segments as measured for $x = 0$ (eqn. (5)) *versus* the electrode potential.

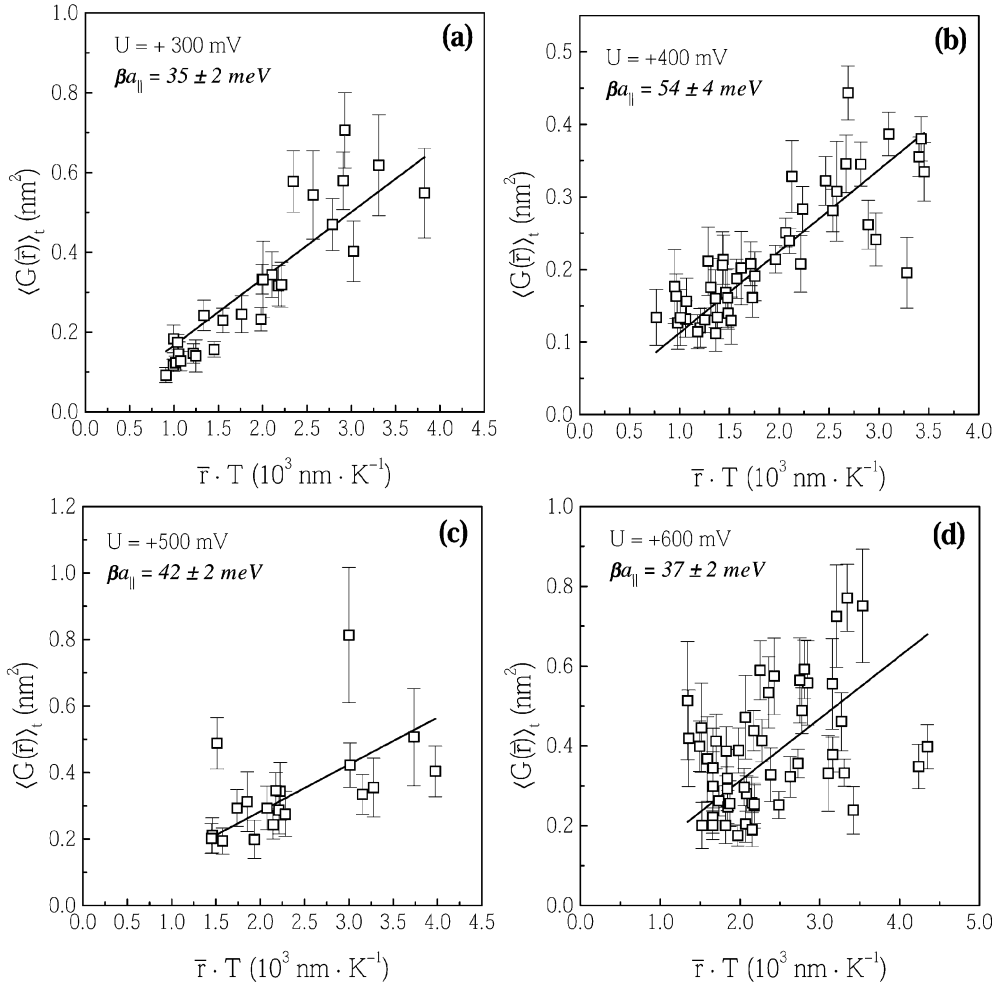

Fig. 5 Measured island shape fluctuation function $\langle G(\bar{r})\rangle_t$ as defined in eqn. (6) for (a) +300 mV, (b) +400 mV, (c) +500 mV and (d) +600 mV *vs.* SCE. See text for discussion.

Table 2 and are plotted in Fig. 7. Similar to the results of the step energy, the kink energy shows a non-monotonic trend.

The application of eqn. (5) to the Au(100) island data was made under the assumption that kinks are merely of monatomic length (*i.e.* $\varepsilon \gg k_B T$) and that the diffusivity b^2 can be replaced by the kink concentration $2a_\perp{}^2 \exp(-\varepsilon/k_B T)$. With kink energies between 31 and 65 meV as obtained here and with $T = 297$ K (corresponding to 26 meV) we may already have reached the limit where the approximation fails. In order to estimate the possible error introduced by this approximation we calculate the diffusivity for kinks of multiple atomic length in a nearest-neighbour model: We associate the energy of kinks of length $na_\perp$ with a formation energy $n\varepsilon$. Then, the diffusivity is given by[57,58]††

$$b^2 = \frac{a_\perp^2}{2\,\sinh^2(\varepsilon/2k_B T)} \tag{7}$$

†† Note the misprint in the formula as given in ref. 36 in eqn. (3.17).

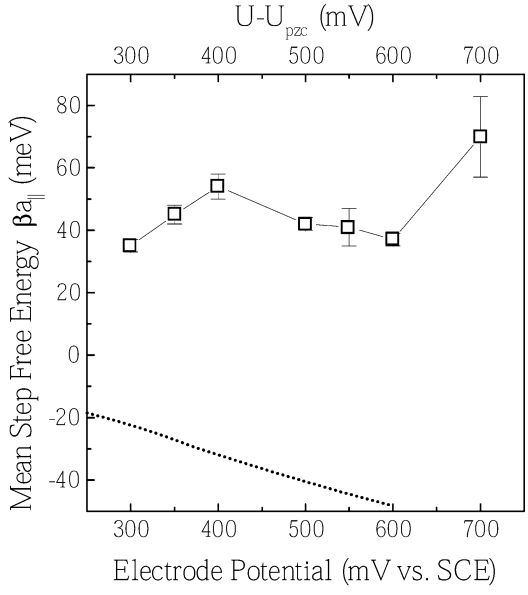

Fig. 6 Plot of the values for the mean step free energy as obtained from $\langle G(\bar{r})\rangle_t$ (Fig. 5) *versus* electrode potential. The dotted line represents the contribution of the line excess charge caused by the step dipole moment to compare in magnitude to the experimental data (see text for discussion).

Using eqn. (7) in eqn. (5) instead, one would get *e.g.* with $yy'' = 0.8005$ (see Table 2; $U = +300$ mV) $\varepsilon = 42$ meV rather than 31 meV. This deviation is outside the error bar of ± 3 meV as given in Table 2. The results for the kink energy using eqn. (7) for the other potentials are also given in Table 2 and are denoted as "ε_{NN}" and are plotted in Fig. 7 as the dashed curve. While the deviation between ε_{NN} and ε is quite noticeable the overall shape of the potential dependence is not affected.

4. Discussion

The fluctuation method used in this work determines the step free energy (line tension) averaged over the angle in a rather particular manner.[50] It can be shown, however, that this average is practically equivalent to the arithmetic average over the angle θ. Fig. 2(b) then instructs us that the arithmetic mean is between 2 and 5% larger than the free step energy of steps oriented along the direction of dense packing. On the other hand the step free energy differs from the step energy (a

Table 2 Data for the slope of the fluctuation function $\langle G(\bar{r})\rangle_t$ and the mean step free energy $\bar{\beta}\, a_{\|}$ along the island perimeter as defined in eqn. (6) and measured from plots as shown in Fig. 5. Using eqn. (5) and the data for the curvature yy'' (mean) as taken from Table 1, the kink energy ε is obtained. The last column denoted as "ε_{NN}" displays values for the kink energy estimated from a nearest-neighbour model to account for kinks of multiple length (see text for discussion).

Electrode potential/mV *vs.* SCE	Slope of $\langle G(\bar{r})\rangle_t/10^{-4}$ nm K^{-1}	$\bar{\beta}a_{\|}$/meV	yy'' (mean)	ε/meV	ε_{NN}/meV
300	1.7 ± 0.1	35 ± 2	0.8005	31 ± 3	42
350	1.3 ± 0.1	47 ± 3	0.6456	44 ± 3	52
400	1.1 ± 0.1	54 ± 4	0.6242	49 ± 4	55
500	1.4 ± 0.1	42 ± 2	0.5878	44 ± 2	51
600	1.6 ± 0.1	37 ± 2	0.6494	38 ± 3	47
700	0.8 ± 0.1	70 ± 13	0.4245	65 ± 10	69

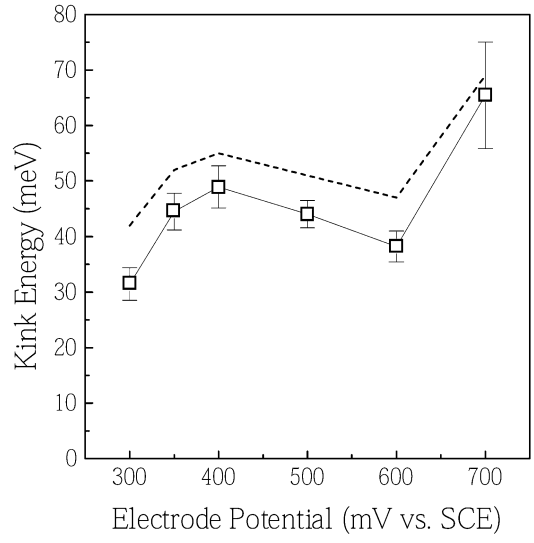

Fig. 7 Plot of the kink energy ε (squares) as determined using eqn. (5) and the data for the mean step free energy (Fig. 6). The dashed line is an estimate of possible corrections to the kink energy due to the influence of kinks of multiple length.

quantity usually calculated in solid state theory) by a phonon contribution and a configurational contribution. In the absence of better knowledge the phonon contribution can be estimated from the reduced co-ordination of the step atoms and the configurational contribution is given by the kink concentration (see ref. 45 for details).

$$a_{\|}\beta(\theta = 0, T) = a_{\|}\beta(\theta = 0, T = 0) - 3k_{\mathrm{B}}T\ \ln(\sqrt{8/7}) - 2k_{\mathrm{B}}T\mathrm{e}^{-\varepsilon_k/k_{\mathrm{B}}T} \tag{8}$$

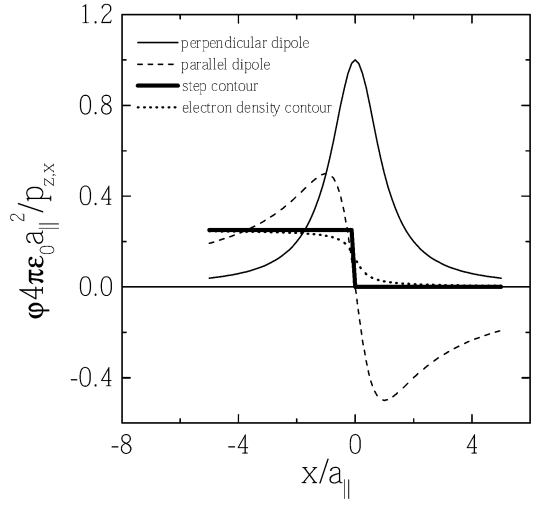

Fig. 8 Step contour and the contour of constant electron charge which follows the step contours smoothly are plotted as a thick solid line and a dotted line, respectively. The dipole moment caused by this "Smoluchowski effect" gives rise to a local variation of the potential. The contributions due to the perpendicular and parallel components of the dipole moment are plotted as thin solid and dashed lines, respectively.

For room temperature and a kink energy of 45 meV the difference between the step free energy and the step energy amounts to 14 meV and is thus by no means small compared to the measured values in this case. This is different from the case of step energies of Cu and Ag in UHV,[45] and this fact should be kept in mind if a comparison with total energy calculations should be attempted in the future. We note further that the kink and step energies are roughly identical (Table 2). The island equilibrium shape is therefore well described by the Ising model.[45,59] Since an analysis of the equilibrium island shape in terms of the Ising model is rather straightforward and requires less extensive data sets for an accurate determination of the Ising parameter, this model could be useful for further studies on the precise potential dependence.

The most striking feature in the experimental data is the non-monotonic shape of the potential dependence. This is contrary to previous observations on the diffusion and dissolution energies on Au(111)[28] and Ag(111).[25] In both studies, the equilibrium step fluctuations on the electrodes were investigated as a function of the potential and a monotonic increase of the fluctuation amplitude was found. The latter was interpreted as a monotonic change in the relevant activation barriers for atomic diffusion.‡‡ A monotonic change in the surface energy upon variation of the surface excess charge and hence the electrode potential was also found in total energy calculations by Bohnen and Kolb.[60] Furthermore, specific adsorption of electrolyte ions at surfaces and at step sites depends monotonically on the potential.[37,61,62] Step energies, in particular step–step interactions have frequently been discussed in the context of surface stress.[63] However, on Au(100) the surface stress is again a monotonic function of the potential,[64,65] and thus not a likely candidate for the cause of the variation of the step energy. Furthermore, elastic energies associated with surface stress are typically small.[63] On the other hand, a non-monotonic change in step edge diffusion as a function of the electrode potential was observed by McHardy *et al.* for Au(111) in perchloric acid.[66] These authors could assign changes in the step edge diffusion to phase transitions of the electrode surface structure related to the specific adsorption of electrolyte ions. In the specific case here, we also found that the step free energy depends on whether the specifically adsorbed sulfate ions were disordered or reveal the ordered superstructure recently reported by Kolb and coworkers.[15,56] In our measurements we made sure, however, that the ordered sulfate adlayer was not present for all the data sets. A model based on adsorbate induced changes in the step energy, not uncommon in ultra-high vacuum surface science, could therefore describe the observed variation with the potential only if one invokes structural changes in the layer of specifically adsorbed sulfate ions to occur locally near or at steps in the potential range of interest. Whether or not such structural changes exist must be left to future investigation, so far no evidence is available, to the best of our knowledge. In any case we consider it as unlikely that the non-monotonic shape of the potential dependence of β and ε is caused by a single effect. Rather a combination of several effects such as specific adsorption at steps and the contribution of a step excess charge could be responsible. In order to obtain some feeling for the magnitude of the effects caused by an excess charge at the steps we discuss the electrostatics of steps in greater detail in the following section. The discussion of electrostatic contributions to the step free energy (*i.e.* the line tension) can be carried forward analogously to the dependence of the surface tension on the electrode potential U. For the surface tension γ one has the Lippmann equation[67]

$$\gamma(U - U_{\mathrm{pzc}}) = \gamma(U_{\mathrm{pzc}}) - \int_{U_{\mathrm{pzc}}}^{U} \tilde{Q}(U')\mathrm{d}U' \tag{9}$$

Here, $\tilde{Q}(U)$ is the surface charge per area (defined in the electric sense as positive for positive voltage) and U_{pzc} is the potential of zero charge. The surface charge can be expressed in terms of the differential capacitance per area $\tilde{C}(U)$ as

$$\tilde{Q}(U') = \int_{U_{\mathrm{pzc}}}^{U'} \tilde{C}(U'')\mathrm{d}U'' \tag{10}$$

‡‡ Note that fluctuations of the infinitely long steps are determined by activation barriers for diffusion and by kink formation energies, fluctuations of closed steps (island edges) only by the line tension.

For small deviations from the potential of zero charge the capacitance $\tilde{C}(U)$ can be expanded in a Taylor-expansion around the pzc. Keeping only the first term one has for the surface tension

$$\gamma(U - U_{\mathrm{pzc}}) = \gamma(U_{\mathrm{pzc}}) - \tfrac{1}{2}\tilde{C}(U_{\mathrm{pzc}})(U - U_{\mathrm{pzc}})^2 \tag{11}$$

Since the surface capacitance is a positive quantity, the surface tension has a maximum at the pzc. This does not necessarily hold for the line tension of a step. The equivalents to eqn. (9) and (11) for the line tension β are, respectively

$$\beta\big(U - U_{\mathrm{pzc}}\big) = \beta\big(U_{\mathrm{pzc}}\big) - \int_{U_{\mathrm{pzc}}}^{U} Q_{\mathrm{step}}(U')\mathrm{d}U' \,, \tag{12}$$

$$\beta(U - U_{\mathrm{pzc}}) = \beta(U_{\mathrm{pzc}}) - \tfrac{1}{2}C_{\mathrm{step}}(U_{\mathrm{pzc}})(U - U_{\mathrm{pzc}})^2 \tag{13}$$

Here, the step charge Q_{step} and the step capacitance C_{step} are defined as integrals over the charge and capacitance per area along a coordinate perpendicular to the step direction minus the same integrals in an area which does not contain a step.

$$Q_{\mathrm{step}} = \lim_{l\to\infty} \int_{-l}^{+l} \tilde{Q}_{\mathrm{with\ step}}(x)\mathrm{d}x - 2l\tilde{Q}_{\mathrm{without\ step}} \tag{14}$$

$$C_{\mathrm{step}} = \lim_{l\to\infty} \int_{-l}^{+l} \tilde{C}_{\mathrm{with\ step}}(x)\mathrm{d}x - 2l\tilde{C}_{\mathrm{without\ step}} \tag{15}$$

Because of the integration C_{step} is a capacitance per step length. A calculation of the step capacitance should be possible in the framework of a Gouy–Chapman model. Such a calculation would involve solving the Poisson–Boltzmann equation with the step geometry as an input. We do not know whether the calculation can be carried out analytically. A numerical calculation should be relatively straightforward, however. We note that the step capacitance need not be positive. Intuition as well as initial rounds in an attempt to calculate the step capacitance numerically show that it is negative. This would mean that the step free energy has a minimum at the pzc! This obviously rather interesting issue will be addressed in a separate publication at a later time.

We now consider a further contribution to the step free energy which arises from the local dipole moment at steps. The dipole moment is due to the well known Smoluchowski effect:[68] Near a step the electron charge density contours follow the step contour only smoothly in order to save kinetic energy at the expense of building up the electrostatic energy associated with the local deviation from neutrality (Fig. 8). The vertical component of the step dipole moment gives rise to a reduction in the work function on vicinal surfaces with regular step arrays and can therefore be measured.[40] The relation between the vertical component of the dipole moment per step atom p_z and the reduction in the work function $\Delta\Phi$ is

$$p_z = \varepsilon_0 a_{\|} L \Delta\Phi \tag{16}$$

Here, ε_0 is the absolute permittivity and L the distance between the steps. Eqn. (16) can either be derived by a formal integration of the dipole potentials, or, straightforwardly by considering a homogeneous distribution of dipoles in the continuum limit. For our considerations here we are interested in the local variation of the potential due to the surface dipole of steps which are assumed to be straight and infinitely long. Defining cartesians perpendicular to the step, along the step, and perpendicular to the surface as x, y, and z, respectively, one obtains for the electrostatic potential caused by the step dipole

$$\phi_s(x,z) = \frac{1}{2\pi\varepsilon_0 a_{\|}}\left(p_z \frac{z}{x^2+z^2} + p_x \frac{x}{x^2+z^2}\right) \tag{17}$$

with p_x the parallel component of the step dipole moment. The form of the potential at a distance of $z = a_{\|}$ is displayed in Fig. 8. Note that the calculation is for a point dipole and is with reference

to the plane $z = 0$! The potential to be added locally to the potential of the electrode is twice the amount. The electrostatic potential gives rise to a local variation in the double layer charge and hence to a local variation in the electric work stored in the double layer capacitor. This variation ΔW_{el} per step length is

$$\Delta W_{el}(U - U_{pzc}) = \int_{-\infty}^{+\infty} dx \int_{0}^{2\phi_s(x,z>0)} \tilde{Q}(U - U_{pzc} + U')dU' \tag{18}$$

In the range of interest here $\varphi_s \ll U - U_{pzc}$, the term $\tilde{Q}(U - U_{pzc} + U')$ can be considered constant and one has for ΔW_{el}

$$\Delta W_{el}(U) = 2\tilde{Q}(U) \int_{-\infty}^{+\infty} \phi_s(x, z > 0)dx \tag{19}$$

The integration can be carried out in closed form. The integral is independent of the distance z, and only the perpendicular dipole moment contributes.

$$\Delta W_{el}(U) = \frac{p_z}{\varepsilon_0 a_{||}} \tilde{Q}(U) \tag{20}$$

Thus, the line tension becomes

$$\beta(U - U_{pzc}) = \beta(U_{pzc}) - \int_{U_{pzc}}^{U} Q_{step}(U')dU' - \frac{p_z}{\varepsilon_0 a_{||}} \tilde{Q}(U - U_{pzc}) \tag{21}$$

The second term is roughly quadratic and the third term roughly linear in the electrode potential. Unless a numerical calculation with the step geometry and the charge distribution at the step would bring up surprises, the electrostatic contribution to the line tension seems to be a smooth function of the potential. It is nevertheless interesting to calculate the magnitude of the electrostatic contribution which can be performed at least for the third term in eqn. (21). The surface charge density per area $\tilde{Q}(U)$ is known for Au(100) in sulfuric acid.[69] The value for the dipole moment could be taken from work function measurements on vicinal surfaces. While such data does not seem to be available for Au(100) vicinals, the work of Besocke *et al.*[40] reports $p_{(111)} = 2.4 \times 10^{-29}$ (A s cm) (corresponding to 0.015 *e* Å) for the A-steps ((111) facets) on Au(111) surfaces. Because of the lower step height on (111) surfaces compared to (100) surfaces this number is considered as a lower limit for the dipole moment on Au(100) steps in vacuum. Inserting this number for the dipole moment one obtains the dotted curve in Fig. 6. The result clearly demonstrates that the electrostatic energy has an appreciable effect on the step energy and should be taken into consideration less cursorily than here in this paper.

Finally, we want to discuss an issue of concern that may be raised when discussing STM results. In studies of atomic motion on surfaces, the problem arises as to how far the results are influenced by the presence of the tunnelling tip. As has been demonstrated in ref. 26, the tunnelling bias may locally induce electrochemical reactions such as metal dissolution. For potentials far from a phase transition it has been shown that moderate tunnelling parameters may prevent an influence of the tip on the analysis of atomic motion at the interface.[26] In the studies presented here we have not performed systematic measurements of the equilibrium island shape for different tunnelling parameters. This would have been an immense task considering that for each variation of the tunnelling parameters we would have to analyse thousands of island shapes to be able to compare statistically comparable data sets. We have therefore used a different procedure to check on a possible tip influence: If the island shape and the shape fluctuations are influenced by the presence of the tip due to changes in atomic motion along the island perimeter one would expect that tip effects would be more efficient for small islands since they contain relatively more periphery atoms. Hence, we checked for possible differences in the island equilibrium shape as a function of the island size and found no measurable deviations in the island shape. In fact, even if there was a small influence of the tip and several atoms were shifted by several lattice spacings whenever the tip scans across an island edge, this influence would hardly be noticeable: Most of the shape fluctuations,

which are up to two orders of magnitude larger, happen during the time the tip scans across a totally different surface region. Hence, when averaging over a large number of individual (not too small) islands one may safely exclude tip influence on the island data, at least on Au(100) as studied here.

5. Summary

We have analysed the equilibrium island shape of monolayer high islands on the Au(100) electrode in sulfuric acid as a function of the electrode potential. From these studies we determine the potential variation of the step and the kink energy. We find values of the order of 35–70 and 31–65 meV, respectively, varying with the electrode potential. The dependence of both the step and the kink energy on the electrode potential is non-monotonic and is presumably caused by a combination of several effects. One component, the contribution of the excess step charge, was discussed in greater detail in terms of a simple model and it was found that the electrostatic contribution to the step free energy is non-negligible. For a more complete understanding further experimental studies with different electrolytes as well as more detailed theoretical investigations which include the adsorption isotherms at step sites are necessary.

Acknowledgement

The skilful preparation of the Au(100) single crystal electrodes by Udo Linke is gratefully acknowledged. We have benefited from helpful discussions with D M Kolb and W Schmickler both from Abteilung für Elektrochemie, Universität Ulm. This work has been partially supported by the Fonds der Chemischen Industrie, Germany.

References

1 R. Sonnenfeld and P. K. Hansma, *Science*, 1986, **232**, 211.
2 H. Liu, F. F. Fan, C. W. Lin and A. J. Bard, *J. Am. Chem. Soc.*, 1986, **108**, 3838.
3 J. Hotlos, O. M. Magnussen and R. J. Behm, *Surf. Sci.*, 1995, **335**, 129.
4 F. Möller, O. M. Magnussen and R. J. Behm, *Electrochim. Acta*, 1995, **40**, 1259.
5 M. S. Zei, K. Wu, M. Eiswirth and G. Ertl, *Electrochim. Acta*, 1999, **45**, 809.
6 G. Staikov and W. J. Lorenz, *Z. Phys. Chem.*, 1999, **208**, 17.
7 U. Schmidt, S. Vinzelberg and G. Staikov, *Surf. Sci.*, 1996, **348**, 261.
8 T. P. Moffat, *J. Phys. Chem. B*, 1998, **102**, 10 020.
9 Z. Shi, S. Wu and J. Lipkowski, *Electrochim. Acta*, 1995, **40**, 9.
10 J. G. Xu and X. W. Wang, *Surf. Sci.*, 1998, **408**, 317.
11 M. Dietterle, T. Will and D. M. Kolb, *Surf. Sci.*, 1995, **342**, 29.
12 M. Dietterle, T. Will and D. M. Kolb, *Surf. Sci.*, 1998, **396**, 189.
13 R. Randler, M. Dietterle and D. M. Kolb, *Z. Phys. Chem.*, 1999, **208**, 43.
14 B. M. Ocko, I. K. Robinson, M. Weinert, R. J. Randler and D. M. Kolb, *Phys. Rev. Lett.*, 1999, **83**, 780.
15 A. Cuesta, M. Kleinert and D. M. Kolb, *Phys. Chem. Chem. Phys.*, 2000, **2**, 5684.
16 D. M. Kolb, *Prog. Surf. Sci.*, 1996, **51**, 109–73.
17 O. M. Magnussen, J. Hotlos, R. J. Behm, N. Batina and D. M. Kolb, *Surf. Sci.*, 1993, **296**, 310.
18 R. J. Nichols, O. M. Magnussen, J. Hotlos, T. Twomey, R. J. Behm and D. M. Kolb, *J. Electroanal. Chem. Interfacial Electrochem.*, 1990, **290**, 21–31.
19 M. S. Zei, G. Lehmpfuhl and D. M. Kolb, *Surf. Sci.*, 1989, **221**, 23.
20 O. M. Magnussen, J. Hageböck, J. Hotlos and R. J. Behm, *Faraday Discuss. Chem. Soc.*, 1992, **94**, 329.
21 J. X. Wang and R. R. Adzic, *J. Electroanal. Chem.*, 1998, **448**, 205.
22 X. Gao, A. Hamelin and M. Weaver, *J. Chem. Phys.*, 1991, **95**, 6993.
23 J. V. Barth, H. Brune, G. Ertl and R. J. Behm, *Phys. Rev. B*, 1990, **42**, 9307.
24 M. Dietterle, T. Will and D. M. Kolb, *Surf. Sci.*, 1995, **327**, L495.
25 M. Giesen, M. Dietterle, D. Stapel, H. Ibach and D. M. Kolb, *Surf. Sci.*, 1997, **384**, 168.
26 M. Giesen, R. Randler, S. Baier, H. Ibach and D. M. Kolb, *Electrochim. Acta*, 1999, **45**, 533.
27 O. M. Magnussen and M. R. Vogt, *Phys. Rev. Lett.*, 2000, **84**, 357.
28 M. Giesen and D. M. Kolb, *Surf. Sci.*, 2000, **468**, 149.
29 S. Baier and M. Giesen, *Phys. Chem. Chem. Phys.*, 2000, **2**, 3675.
30 S. Baier, S. Dieluweit and M. Giesen, *Surf. Sci.*, 2002, **502–503**, 463.
31 S. Dieluweit and M. Giesen, *J. Phys. Condens. Matter*, 2002, **14**, 4211.
32 D. M. Kolb, R. Ullmann and J. C. Ziegler, *Electrochim. Acta*, 1998, **43**, 2751.

33 P. Broekmann, M. Wilms, M. Kruft, C. Stuhlmann and K. Wandelt, *J. Electroanal. Chem.*, 1999, **467**, 307.
34 N. Hirai, K. Watenabe, A. Shiraki and S. Hara, *J. Vac. Sci. Technol. B*, 2000, **18**, 7.
35 N. Hirai, K. Watanabe and S. Hara, *Surf. Sci.*, 2001, **493**, 568.
36 M. Giesen, *Prog. Surf. Sci.*, 2001, **68**, 1.
37 W. Schmickler, *Annu. Rep., Sect. C*, 1999, **95**, 117.
38 T. Dretschkow and T. Wandlowski, *Ber. Bunsen-Ges. Phys. Chem.*, 1997, **101**, 749.
39 E. Budevski, G. Staikov and W. J. Lorenz, *Electrochemical Phase Formation and Growth*, VCH, Weinheim, 1996.
40 K. Besocke, B. Krahl-Urban and H. Wagner, *Surf. Sci.*, 1977, **68**, 39.
41 A. Popov, N. Dimitrov, T. Vitanov and D. Kashchiev, *Electrochim. Acta*, 1995, **40**, 1495.
42 X.H. Xia, R. Schuster, V. Kirchner and G. Ertl, *J. Electroanal. Chem.*, 1999, **461**, 102.
43 G. Wulff, *Z. Kristallogr. Mineral.*, 1901, **34**, 449.
44 M. Wortis, in *Chemistry and Physics of Solid Surfaces*, ed. R. Vanselow and R. Howe, Springer, New York, 1988, p. 367.
45 M. Giesen, C. Steimer and H. Ibach, *Surf. Sci.*, 2001, **471**, 80.
46 N. C. Bartelt, T. L. Einstein and E. D. Williams, *Surf. Sci.*, 1990, **240**, L591.
47 H.-C. Jeong and E. D. Williams, *Surf. Sci. Rep.*, 1999, **34**, 171.
48 S. V. Khare and T. L. Einstein, *Phys. Rev. B*, 1996, **54**, 11 752.
49 D. C. Schlößer, L. K. Verheij, G. Rosenfeld and G. Comsa, *Phys. Rev. Lett.*, 1999, **82**, 3843.
50 C. Steimer, M. Giesen, L. Verheij and H. Ibach, *Phys. Rev. B*, 2001, **64**, 085416.
51 M. Giesen and S. Baier, *J. Phys. Condens. Matter*, 2001, **13**, 5009.
52 A. S. Dakkouri, R. Randler and D. M. Kolb, in *Proceedings of the Symposium on: The Electrochemical Double Layer*, ed. C. Korzeniewski and B. E. Conway, The Electrochemical Society, Pennington, NJ, 1997.
53 A. Dakkouri, PhD Thesis, 1996.
54 D. M. Kolb, *Prog. Surf. Sci.*, 1996, **51**, 109.
55 C. E. Bach, R. J. Nichols, W. Beckmann, H. Meyer, A. Schulte, J. O. Besenhard and P. D. Jannakoudakis, *J. Electrochem. Soc.*, 1993, **140**, 2181.
56 M. Kleinert, A. Cuesta, L. A. Kibler and D. M. Kolb, *Surf. Sci.*, 1999, **430**, L521–6.
57 B. S. Swartzentruber, Y.-W. Mo, R. Kariotis, M. G. Lagally and M. B. Webb, *Phys. Rev. Lett.*, 1990, **65**, 1913.
58 M. Poensgen, J. F. Wolf, J. Frohn, M. Giesen and H. Ibach, *Surf. Sci.*, 1992, **274**, 430.
59 R. K. P. Zia and J. E. Avron, *Phys. Rev. B*, 1982, **25**, 2042.
60 K. P. Bohnen and D. M. Kolb, *Surf. Sci.*, 1998, **407**, L629–32.
61 J. Lipkowski, Z. Shi, A. Chen, B. Pettinger and C. Bilger, *Electrochim. Acta*, 1998, **43**, 2875.
62 I. R. d. Moraes and F. C. Nart, *J. Electroanal. Chem.*, 1999, **461**, 110.
63 H. Ibach, *Surf. Sci. Rep.*, 1997, **29**, 193.
64 C. Bach, M. Giesen, H. Ibach and T. L. Einstein, *Phys. Rev. Lett.*, 1997, **78**, 4225.
65 H. Ibach, C. E. Bach, M. Giesen and A. Grossmann, *Surf. Sci.*, 1997, **375**, 107.
66 R. McHardy, W. H. Haiss and R. J. Nichols, *Phys. Chem. Chem. Phys.*, 2000, **2**, 1439.
67 W. Schmickler, *Interfacial Electrochemistry*, Oxford University Press, New York, 1996.
68 R. Smoluchowski, *Phys. Rev.*, 1941, **60**, 661.
69 D. M. Kolb and J. Schneider, *Surf. Sci.*, 1985, **162**, 764.